

PRS-Med: Position Reasoning Segmentation with Vision-Language Model in Medical Imaging

Quoc-Huy Trinh^{1,3,6} Minh-Van Nguyen^{2,6} Jun Peng⁵ Ulas Bagci³ Debesh Jha⁴

¹Aalto University ²Denmark Technical University ³Northwestern University

⁴University of South Dakota ⁵Chongqing University of Posts and Telecommunications ⁶SpexAI GmbH

huy.trinh@aalto.fi, s242503@dtu.dk, zeng.cqupt@gmail.com

ulas.bagci@northwestern.edu, debesh.jha@usd.edu

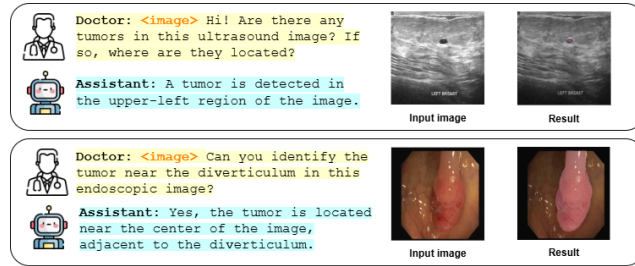


Figure 1: Example interaction between the doctor and proposed assistant model. Given a natural language prompt about a tumour and its location, along with an input image, the assistant returns a segmentation result and a spatially grounded textual description.

Abstract

Recent advancements in prompt-based medical image segmentation have enabled clinicians to identify tumors using simple input like bounding boxes or text prompts. However, existing methods face challenges when doctors need to interact through natural language or when position reasoning is required - understanding spatial relationships between anatomical structures and pathologies. We present *PRS-Med*, a framework that integrates vision-language models with segmentation capabilities to generate both accurate segmentation masks and corresponding spatial reasoning outputs. Additionally, we introduce the *MMRS dataset* (Multimodal Medical in Positional Reasoning Segmentation), which provides diverse, spatially-grounded question-answer pairs to address the lack of position reasoning data in medical imaging. PRS-Med demonstrates superior performance across six imaging modalities (CT, MRI, X-ray, ultrasound, endoscopy, RGB), significantly outperforming state-of-the-art methods in both segmentation accuracy and position reasoning. Our approach enables intuitive doctor-system interaction through natural language, facilitating more efficient diagnoses. Our dataset pipeline, model, and codebase will be released to foster further research in spatially-aware multimodal reasoning for medical applications.

1 Introduction

In medical settings, doctors typically perform diagnoses by observing potential tumour locations to assess tissue conditions. This makes the *position reasoning and segmentation* essential tasks for supporting early and accurate diagnosis. In the age of the medical assistant agents, several Vision

Large Language Models (VLMs), including LLaVA-Med [27], Med-MoE [23], HuatuoGPT [7], and MedVLM-R1 [36] have been proposed to assist in tumour detection from medical imaging and provide reasoning about the tumours. Although these models have demonstrated promising capabilities in reasoning and accurately identifying tumours within medical images, there is a practical challenge arises as doctors often **seek to identify unknown tumour locations through implicit questions or conversational interactions**. Moreover, during the diagnosis process, the result that doctors need to predict the status of the anatomy is the location of the tumour in the medical images, not only the information about the tumour. This is the reason why position reasoning segmentation becomes critical to help the doctor in recognizing the tumours, thereby facilitating more effective diagnosis and treatment. Additionally, this technique can help the clinics to create an automated screening system, thus reducing the cost of doing it manually.

Recently, in the natural image domain, the challenge of reasoning for segmentation has been addressed by several works such as LISA [26], LLM-SEG [48], and SEGLLM [52]. These models have achieved notable success in enhancing object reasoning and accurately identifying object positions via segmentation, and provide simple reasoning about the object. However, these models **do not explicitly address position reasoning and are not well-trained on medical imaging data**. Thus, applying this model to medical imaging faces several difficulties.

Inspired by recent methods like SpatialVLM [6], SpatialRGPT [9], and LocVLM [38], which demonstrate the promising initial results in position understanding and reasoning, we aim to address the current challenge in developing an intelligent medical image assistant. In this paper, we propose **PRS-Med: Position Reasoning Segmentation through Vision-Language Models** for medical imaging. This method aims to perform position-reasoning segmentation from the simple question or command input, via the Multimodal-LLM (Vision Language Model) that incorporates the vision feature from the SAM image encoder. The model can describe the position of the tumour in text, recognize and point out the tumours inside the medical image through the segmentation mask. As a result, PRS-Med is an intelligent assistant that can interactively answer questions from the doctor and visually indicate the tumour position in an interpretable manner.

In summary, our contributions are in four folds:

- We propose the **PRS-Med**, a novel position reasoning model that integrates *multimodal vision-language learning with a lightweight TinySAM image encoder* to perform spatially-aware tumour segmentation via the implicit natural language prompt.
- We construct and release the *Multimodal Medical in Positional Reasoning Segmentation (MMRS)* dataset pipeline, which can construct a comprehensive positioning benchmark pipeline, designed to generate diverse, spatially grounded question-answer pairs and address the lack of datasets and evaluation tools for position reasoning in the field of medical imaging domain.
- We conduct extensive quantitative and qualitative experiments across six modalities (CT, MRI, X-ray, ultrasound, endoscopy, and RGB), demonstrating PRS-Med surpasses state-of-the-art (SOTA) segmentation and reasoning models in both accuracy and generalization.
- We open-source the dataset pipeline, model, and codebase to the community, which facilitates the development of the spatially-aware multimodal LLMs in medical imaging.

The rest of this paper is organized as follows: in Section 2, we briefly review existing methods related to this research. Then we introduce position reasoning and the segmentation dataset preparation pipeline in Section 3. Afterward, we introduce our proposed model, PRS-Med, in Section 4, and the position reasoning benchmark for Medical Imaging in Section 5. Experiment setups are in Section 6. Results of the model assessment is mentioned in Section 7 Finally, we present the conclusion in Section 8.

2 Related Work

Reasoning Image Segmentation: Recent advancements in reasoning segmentation have begun to integrate high-level reasoning, particularly through the use of the Multimodal-LLMs. Notable works in the domain include LISA [26], LLM-Seg [49], and SegLLM [53], which include a special [SEG] token used to extract segmentation-specific embeddings from the model. However, applying this

method for the position reasoning is challenging due to the limitations in the annotated data and the difficulty of adapting to medical-specific vocabulary. To address this limitation, in our design of PRS-Med, we integrate the global token embeddings from the Multimodal-LLM with the visual features of medical images, enabling effective position-aware segmentation.

Medical Image Segmentation: Traditional Medical image segmentation has long relied on fully supervised CNN-based architectures like U-Net [39] and its variant such as ResUNet++ [22], nnu-net [19], DoubleUNet [20], TransResUNet [45], and Swin-UNet [5]. More recently, several promptable segmentations have emerged as a response to the growing demand for interactive and context-aware medical AI. MedSAM [33], SAM-Med2D [12] adapts the Segment Anything Model (SAM) [24] to medical settings, supporting box- and point-prompted segmentation. However, MedSAM and SAM-Med2D still lack semantic understanding of positional cues within free-form text. In contrast, BiomedParse [58] directly uses text prompts to infer object shapes and positions, learning implicit position priors. Despite its novelty, BiomedParse does not couple segmentation with contextual reasoning, nor does it support implicit or conversational prompts beyond class names. PRS-Med integrates position reasoning with segmentation, enabling an interactive framework that responds to contextual questions and generates both position reasoning outputs and corresponding segmentation masks.

Multimodal-LLM in Medical Imaging: Multimodal large language models (MLLMs) have recently shown promising results in medical image reasoning tasks. Prominent methods such as Med-Flamingo [35], Med-MoE [35], GSCo [17], HuatuoGPT [7] and MedVLM-R1 [36], are built upon vision and Language models like LLaVA [30], Qwen2-VL [50], and Multimodal Llama [46] through the training technique via visual instruction tuning or reinforcement learning methods. Despite their promising results, these models struggle with medical image segmentation, which is a critical task for accurate disease diagnosis. Moreover, they also inherit spatial reasoning limitations from their Multimodal-LLMs which is observed in the prior works such as SpatialVLM [6], Loc-VLM [38], and Spatialrgpt [9]. To address these challenges, we propose PRS-Med, which extends MLLM capabilities by enabling accurate segmentation and enhancing position reasoning for medical imaging applications.

3 Position Reasoning Dataset Preparation

The research community has proposed several methods for constructing datasets to support multimodal reasoning, such as LAION [40], and LLaVA [30], which rely on either human annotators or large language models (LLMs) for labeling. However, these approaches face significant challenges when applied to the medical domain, particularly in positional reasoning segmentation, due to the limited availability of high-quality specialized datasets and the critical requirement for accuracy. Accuracy is especially critical in healthcare, where incorrect information can have serious consequences. Moreover, manual annotation is both time-consuming and costly, making it difficult to scale. To address these issues, we propose a novel method that leverages the logical capabilities and text generation power of LLMs. Specifically, the LLM is used to generate templated sentences that incorporate positional information extracted directly from the ground truth segmentation masks. This approach enhances dataset diversity, reduces hallucination during pseudo-data generation, and lowers the overall cost by minimizing the need for repeated API calls or hosting LLMs. Figure 2 illustrates the flow of our dataset creation pipeline to serve the positional reasoning segmentation task of medical imaging.

Our dataset creation is including two stages, the first stage is **Dictionary preparation**, where we prepare the template for the question and answer, and the second stage is the **Data creation**, where we will do the mapping and combine the position, modality information to the template.

Regarding the first stage, we prepare samples of the questions and answers as following be the template for the dictionary generation:

1. Question: Where is the tumour position in the <image type> medical image?
2. Answer: There is a <tumour name> in the <position>

To begin, we leverage a large language model—specifically ChatGPT—to generate 50 question-and-answer templates based on the mentioned question-answer pair for training and 5 for testing. These templates are carefully crafted using detailed prompts to ensure that, when combined with the tumour name and positional information, the resulting sentences are coherent and contextually appropriate.

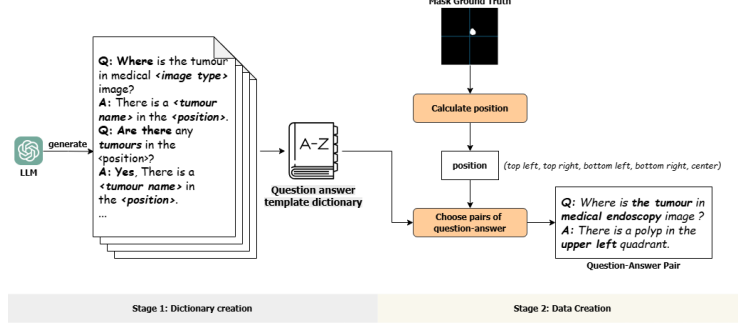


Figure 2: Position reasoning dataset question-answer pair creation consists of two stages: (1) dictionary creation, which stores question-answer templates; and (2) data generation, which produces question-answer pairs using positional information extracted from segmentation masks.

In the second stage, we extract positional information from the segmentation mask. Given a binary mask X_{mask} , we first derive the bounding box $\{x, y, w, h\}$, representing the location of the tumour within the image. From this, we calculate the center point of the tumour as $x_{\text{center}} = \{x + \frac{w}{2}, y + \frac{h}{2}\}$. Next, we divide the image into four quadrants—top left, top right, bottom left, and bottom right—as illustrated in Figure 2. Based on the location of x_{center} , we determine which quadrant the tumour lies in and assign it a corresponding label. In addition to handling cases where tumours are located near the image center, we also compute the distance between x_{center} and the geometric center of the image. If this distance falls below a predefined threshold, we label the tumour as being near the center. Finally, we integrate the extracted positional information with the question-and-answer templates to generate the final dataset of spatially grounded tumour descriptions. As a result, of this dataset pipeline, we release the *pseudo-position reasoning segmentation dataset*, which is used for training the Position Reasoning Medical Image segmentation.

4 PRS-Med

Overall Architecture: The primary goal of PRS-Med is to perform position reasoning segmentation, enabling the model to explain the location of tumours in an image along with relevant medical information. Additionally, the segmentation head allows the model to perform tumour segmentation within the image using a single prompt. The overall architecture is illustrated in Figure 3. Different with the reasoning segmentation of the natural image as LISA [26], in our work, we leverage the full token embedding sequence instead of add a special token [SEG] due to the limitations of the training data, which make the model difficult to learn the new vocabulary.

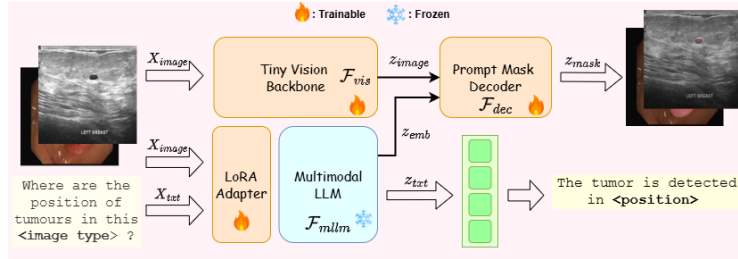


Figure 3: The architecture of PRS-Med comprises three primary components: (1) the Tiny Vision Backbone, (2) the Prompt Mask Decoder, and (3) the Multimodal-LLM. The framework accepts two input modalities: an image and a text-based prompt (e.g., a question). The image is processed through a vision encoder, while the prompt is embedded via a LoRA-adapted Multimodal-LLM. The fused representations are used to produce two outputs: a segmentation mask for the tumor regions, and a textual description specifying the tumor’s location.

This framework consists of four main modules. The first is the Vision-Language Model; in our case, we use LLaVA-Med [27], as it is a well-trained Multimodal-LLM for the medical dataset,

which we can benefit from its domain of expertise. The second module is the Tiny SAM image encoder, employed from TinySAM [41], which is used to encode the input image. The third module is the Decoder, which includes a fusion component that combines image features from the SAM image encoder with the vision-language embeddings from the Medical Vision-Language Model to generate the final segmentation mask. In addition, we include a Language Model Head to perform the reasoning task.

During training, due to the challenges of fine-tuning the full LLaVA-Med model, we apply Low-Rank Adaptation (LoRA) [18] to enable the model to effectively learn position reasoning information from our prepared dataset.

Vision Backbone: The primary objective of the vision backbone is to extract pixel-level features from medical images to support conditional segmentation. For this purpose, we adopt the image encoder from TinySAM [41], which is based on the lightweight TinyViT architecture [56]. This design enables efficient image encoding while reducing computational resource requirements.

Given a batch of b input images $X_{image} \in \mathbb{R}^{b \times 3 \times W \times H}$, the images are processed through a tiny vision transformer model \mathcal{F}_{vis} , consisting of approximately four transformer layers, to produce an image representation embedding $z_{image} \in \mathbb{R}^{b \times 256 \times \frac{W}{16} \times \frac{H}{16}}$. This encoder extracts dense visual features z_{image} , which are used for the segmentation task. During training, the encoder is kept unfrozen to allow it to adapt to the medical image domain, thereby improving segmentation performance. The reason for the design choice of this TinyViT-based vision backbone is detailed in Section 6.

By leveraging pre-trained weights from the TinySAM image encoder, our model can better adapt to the medical domain without initializing weights from scratch, which contributes to improved segmentation outcomes.

Multimodal-LLM: Most current Multimodal-LLM backbones applied to the medical domain—such as Flamingo [2], LLaVA [30], Qwen-VL [51], and InternVL [8]—demonstrate strong reasoning capabilities. However, they generally lack the ability to generate masks for visual recognition tasks and struggle to comprehend positional information, such as the position of objects within an image. Notably, embeddings from the final layer of these multimodal LLMs have proven highly valuable in various robotics applications, as demonstrated in works like TinyVLA [55], RoboMamba [31], and Groot-N1 [4]. Inspired by these insights, we adopt a multimodal LLM design in this module to serve both as a feature extractor for conditioning the masked decoder and as a component for position reasoning. Different with LISA [26] (the reasoning segmentation approach in the natural image), when they create a new token id for segmentation, in this work, we propose a method that leverages directly the joint embedding from the Multimodal-LLM, which can reduce the computation cost in the training for adapting the new vocabulary set.

To generate the Multimodal-LLM embedding $z_{emb} \in \mathbb{R}^{b \times l \times 4096}$ (where l is the token length), and the reasoning output $z_{txt} \in \mathbb{R}^{b \times l}$ from the input image $X_{image} \in \mathbb{R}^{b \times 3 \times w \times h}$ and input text $X_{txt} \in \mathbb{R}^{b \times l \times d}$ (where d is the vocabulary size), we define F_{mllm} as a parametric function implemented using LLaVA-Med [27]. The complete process of the model can be described as follows:

$$z_{emb} = \mathcal{F}_{mllm}(X_{image}, X_{txt}) \quad (1)$$

$$z_{txt} = p(z_{txt}|X_{image}, X_{txt}) = \prod_{i=1}^l p_{\theta}(z_{txt}^i|X_{image}, X_{txt}^{i-1}) \text{ with } 1 < i < l \quad (2)$$

where θ is the trainable parameter. In our case, θ is from the parameter of the parametric function F_{mllm} , which is the weight of the LLaVA-med model.

During training, due to the high computational cost associated with fully supervised fine-tuning of the LLaVA-Med model, we employ the LoRA method [18] as an adapter. This approach allows the model to learn reasoning capabilities from the our generated position medical reasoning dataset while adapting to generate meaningful embeddings for the mask decoder. The selection of LoRA hyperparameters is detailed in Section 6.

Prompt Mask Decoder: The goal of this module is to predict the segmented mask from two inputs are medical images representation feature z_{image} and the embedded image-text prompt z_{emb} from the Multimodal-LLM. For more detailed visualization of the overall decoder, it is shown in Figure 5 of Appendix A.5.

In the Fusion module, given the image representation from the vision encoder, denoted as $z_{\text{image}} \in \mathbb{R}^{b \times 256 \times 16 \times 16}$, and the conditioning input from the Multimodal LLM, denoted as $z_{\text{emb}} \in \mathbb{R}^{b \times l \times 4096}$, the overall fusion process is formalized in Equation 3 and Equation 4.

$$z_{\text{fused}} = SA(\sigma(\frac{\mathcal{F}_{\theta_1}^{\text{proj}}(z_{\text{image}})\mathcal{F}_{\theta_2}^{\text{proj}}(z_{\text{emb}})^T}{\sqrt{d_k}}))\mathcal{F}_{\theta_2}^{\text{proj}}(z_{\text{emb}})) \quad (3)$$

$$z_{\text{fused}} = z_{\text{fused}} + z_{\text{image}} \quad (4)$$

where d_k is the scaling value, $SA(\cdot)$ is the Self-Attention layer, and $\sigma(\cdot)$ is the softmax function. First, the image representation z_{image} is reshaped to a new form $z_{\text{image}} \in \mathbb{R}^{b \times (16 \times 16) \times 256}$ to enable interaction with the embedding $z_{\text{emb}} \in \mathbb{R}^{b \times l \times 4096}$ from the Multimodal LLM. As shown in Equation 3, two projection layers, $\mathcal{F}_{\theta_1}^{\text{proj}}$ and $\mathcal{F}_{\theta_2}^{\text{proj}}$, are applied to project both features into a shared latent space of dimension 256. This alignment allows effective fusion through a cross-attention mechanism, which integrates the image features with the multimodal embeddings. The choice of cross-attention is motivated by the dynamic length of the z_{emb} sequences, making it a more flexible and suitable alternative to simple addition or concatenation. Following the fusion, a self-attention layer is employed to model the internal dependencies within the target sequence. The resulting fused representation, $z_{\text{fused}} \in \mathbb{R}^{b \times (16 \times 16) \times d}$, is then reshaped to $\mathbb{R}^{b \times 256 \times 16 \times 16}$. Finally, as described in Equation 4, a skip connection is introduced to preserve gradient flow and mitigate the vanishing gradient problem during training.

In the Mask Prediction module, the input z_{fused} is passed through a stack of transposed 2D convolutional layers, each followed by Batch Normalization and ReLU activation. This series of operations progressively upsamples z_{fused} to produce the final segmentation output $z_{\text{mask}} \in \mathbb{R}^{b \times 1 \times 1024 \times 1024}$.

Objective Function: This model is trained end-to-end by using the segmentation loss (\mathcal{L}_{seg}) and text generation loss $\mathcal{L}_{\text{text}}$. The overall objective function is depicted in Equation 5.

$$\mathcal{L} = \lambda_{\text{seg}}\mathcal{L}_{\text{seg}} + \lambda_{\text{text}}\mathcal{L}_{\text{text}} \quad (5)$$

where λ_{seg} and λ_{text} shows the importance of each loss in the overall framework.

Regarding \mathcal{L}_{seg} , we employ a combination of Binary Cross-Entropy and Dice loss [43], which is a common choice in image segmentation tasks. For $\mathcal{L}_{\text{text}}$, we use the Categorical Cross-Entropy (CE) loss. Let \hat{y}_{mask} denote the ground truth mask and z_{mask} the predicted mask; similarly, let \hat{y}_{text} be the ground truth token index sequence and z_{text} the predicted text logits. Equations 6 and 7 illustrate the formulations of the aforementioned loss functions.

$$\mathcal{L}_{\text{seg}} = \mathcal{L}_{\text{BCE}}(\hat{y}_{\text{mask}}, z_{\text{mask}}) + \mathcal{L}_{\text{dice}}(\hat{y}_{\text{mask}}, z_{\text{mask}}) \quad (6)$$

$$\mathcal{L}_{\text{text}} = \mathcal{L}_{\text{CE}}(\hat{y}_{\text{text}}, z_{\text{text}}) \quad (7)$$

By employing this objective function, PRS-Med can simultaneously learn position reasoning while also learn to perform segmentation. Notably, training the segmentation task alongside position reasoning allows the segmentation loss to serve as feedback for the position reasoning component, thereby enhancing the overall performance of the position reasoning task.

5 Position Reasoning Benchmark

Position reasoning is a challenging task, as positional content can be represented in various ways. This variability makes the benchmark difficult to solve using purely logic-based methods, so it is necessary for the human evaluation to verify the results, which is costly. To address this challenge, we propose a benchmark method based on an ensemble of agents. Specifically, we leverage two large language models—Qwen 3 [57], LLaMA 3.1 [16] to evaluate the predicted answers by reasoning about positional content. Our assumption for this benchmark is that the Large Language Model has a strong ability to compare the context meaning of two sentences, so if we can leverage this ability to make it compare the predicted sentence with the ground-truth, we can automate the benchmark on a large scale of data. Moreover, the ensemble results can reduce the bias of 1 model on the overall result.

In our benchmark setup, we define a set of two agents $A = \{a_1, a_2\}$. For each agent, we design three different prompts that follow the chain-of-thought [54] technique and instruct the model to return in the yes/no format. These prompts are applied to each pair (P_i, G_i) in the set B , prompting the model to determine whether the predicted answer is similar to the ground truth. Each "yes" answer is awarded one point, while "no" answers receive zero. The prompts used in the benchmark are described in Appendix A.3. The overall result for each agent is calculated by taking the average and getting the standard deviation. The overall result is calculated by the mean of the accuracy results from two agents

By using this ensemble-based approach, we reduce the bias introduced by relying on a single LLM, as done in previous works, which often results in a high risk of benchmark bias.

6 Experimental Setup

Dataset: As mentioned in Section 3, our training dataset is constructed by combining several medical data sources images with generated question-answer annotations for 6 different types of images are ultrasound, MRI, RGB image, CT Image, Xray, and endoscopy images as these are the popular image types, which is mentioned by Biomedparse [59]. All of the datapoints are collected BUSI [1], BrainMRI [10, 11], ISIC [14], LungCT [25], LungXray [13, 25], Kvasir-SEG [21], and ClinicDB [3]. For the train and test split, we follow the original split from the dataset source to ensure the fair comparison. Furthermore, to increase the difficulty and better evaluate generalization, particularly for polyp tissue segmentation, we augment the test set with additional unseen data from CVC300 [47], ETIS [42], and ColonDB [44], alongside the test splits from Kvasir-SEG and ClinicDB. This strategy allows for a more rigorous assessment of our method’s generalization performance. More detail of the dataset is discussed in the appendix.

Implementation Details: In our implementation, experiments were conducted using an H100 80GB GPU. The model was trained for 20 epochs, requiring approximately 24 GPU hours with a batch size of 8. We employed the AdamW optimizer with a learning rate of 1×10^{-4} , and the best checkpoint was selected at epoch 18 based on validation performance. For the LoRA hyperparameter of the Multimodal-LLM, we set the rank of LoRA is 16, alpha value as the same, with the dropout value is 0.05. The LoRA weight is initialized following a uniform distribution.

Comparison Baseline: To compare our work with SOTA methods, we do the comparison on two tasks are the **segmentation task** and the **position reasoning** task. For the Segmentation task, we compare our methods with the Foundation Segmentation model of medical imaging, such as SAM-Med 2D [60] (2024), and Biomedparse [59] (2024), and the reasoning segmentation model, which is reproduced on our dataset is LISA [26] with two versions are 7B and 13 B. Regarding the SAM model in medical imaging, there is a challenge that most medical segmentation model is based on the box prompt. For this reason, we leverage the Grounding Dino [32] as the text understanding model to extract the boxes coordinate for the segmentation task. In the Reasoning task, due to lack of method done reasoning segmentation, we reproduce the fine-tuning process on our dataset for the Multimodal-LLM for medical image, which includes LLaVA-Med [27] (2024), HuatuoGPT-Vision [7] (2024), and MedVLM-R1 [36] (2025) to do the reasoning benchmark. In all of the comparisons, we try to reproduce the best-practice hyperparameter for each method for the fairest comparison.

Evaluation Metric: For the evaluation, we use the mDice, and mIoU to benchmark the segmentation results, as the standard of the medical segmentation task. In terms of the reasoning task, we evaluate through the accuracy metric.

7 Experimental Result

7.1 Qualitative results

Segmentation Results To evaluate the overall performance of our method against SOTA segmentation approaches, we compare it with several prior works. Table 1 presents results on radiology images of different tissue types, specifically Breast and Brain, and Lung-related radiology images in both CT-Scans and X-rays. Table 2 demonstrates the performance of our method on endoscopic and RGB images for polyp detection and skin cancer segmentation, respectively.

Method	Breast Ultrasound		Brain MRI		Lung CT-Scan		Lung X-ray	
	mDice \uparrow	mIoU \uparrow	mDice \uparrow	mIoU \uparrow	mDice \uparrow	mIoU \uparrow	mDice \uparrow	mIoU \uparrow
G-Dino + SAM-Med2D [34]	0.515	0.441	<u>0.667</u>	<u>0.625</u>	0.540	0.392	0.401	0.300
Biomedparse [59]	<u>0.783</u>	<u>0.698</u>	0.294	0.245	0.088	0.061	0.972	0.949
LISA-7B [26]	0.299	0.246	0.478	0.402	0.478	0.402	0.179	0.122
LISA-13B [26]	0.526	0.441	0.124	0.076	<u>0.656</u>	<u>0.528</u>	0.664	0.535
PRS-Med	0.817	0.729	0.803	0.757	0.968	0.943	0.969	0.942
<i>vs previous works</i>	+0.034	+0.031	+0.136	+0.132	+0.428	+0.551	-0.003	-0.007

Table 1: Qualitative results of **PRS-Med** on the radiology images across four tissue types. The highest score in each column is shown in **bold**, and the second highest is underlined.

Method	Polyp Endoscopy		Skin RGB Image	
	mDice \uparrow	mIoU \uparrow	mDice \uparrow	mIoU \uparrow
G-Dino + SAM-Med2D [34]	0.488	0.418	0.237	0.171
Biomedparse [59]	<u>0.824</u>	<u>0.774</u>	0.924	0.867
LISA-7B [26]	0.241	0.202	0.464	0.368
LISA-13B (Llama 2 based) [26]	0.312	0.247	0.643	0.536
PRS-Med	0.843	0.791	0.875	0.799
<i>vs previous works</i>	+0.019	+0.017	-0.049	-0.068

Table 2: Qualitative results of **PRS-Med** on endoscopy and RGB skin lesion image. The highest score in each column is shown in **bold**, and the second highest is underlined.

As shown in the quantitative results, our method outperforms the second-best model, LISA-13B, across four different modalities: Breast Ultrasound, Lung CT-Scan, Lung X-ray, Polyp Endoscopy superior performance in both Dice score and mIoU. Although there is a slight performance gap in the **Brain MRI** and Skin RGB Image modality, our method still demonstrates strong generalization across a wide range of medical imaging tasks, which can demonstrate the effectiveness of our method in solving this problem.

Comparison with the methods based on the Grounding DINO combined with Med-SAM, our model shows the improvement due to the better attribution to the use of a Multimodal LLM, which more effectively represents user queries in a joint embedding space. This enhances the quality of the embeddings and boosts segmentation performance through stronger reasoning capabilities.

In terms of the comparison with other SOTA reasoning-based segmentation methods, our approach achieves better results thanks to the domain expertise embedded in our Multimodal LLM. This domain adaptation improves the representation of medical image features, leading to more accurate segmentation. While LISA-7B and LISA-13B are based on larger, more extensively pre-trained Multimodal LLMs, their limited understanding of medical-specific visual features results in weaker performance in this domain.

Position Reasoning results To assess the performance of the PRS-Med, we do the evaluation on the position reasoning accuracy with SOTA methods in the Multimodal-LLM for medical images, which is depicted in Table 3. As the illustrated results, our method surpasses previous Multimodal-LLM model in the position reasoning task. These results indicate that our Multimodal-LLM model, which also has the ability in doing segmentation can help it improve its position reasoning ability.

Method	Qwen Benchmark	Llama 3.1 Benchmark	Final result
LLaVA-Med [27]	0.426 (\pm 0.006)	0.412 (\pm 0.008)	0.419
HuatuoGPT-Vision [7]	0.450 (\pm 0.001)	0.424 (\pm 0.003)	0.437
MedVLM-R1 [36]	0.217(\pm 0.002)	0.295 (\pm 0.007)	0.256
PRS-Med	0.509 (\pm 0.007)	0.556 (\pm 0.004)	0.533
<i>vs previous works</i>	+0.059	+0.132	+0.096

Table 3: Qualitative results of **PRS-Med** on position reasoning with SOTA multimodal LLMs.

Qualitative analysis In Figure 4 of Appendix A.4, we present qualitative visualizations that highlight the improvements achieved by PRS-Med. The results clearly show that PRS-Med outperforms all previous methods in segmentation performance, consistently generating complete masks with the lowest loss. These improvements are attributed to the informative feature extraction enabled by our lightweight vision encoder, as well as the effectiveness of the fusion module. Overall, the results provide strong evidence for the promise of our approach.

7.2 Ablation Study

To assess the choice of the module in our framework, we conduct several experiments to assess the performance and the limitations of each module. The experiments are conducted in the same training and testing dataset with the benchmark. Regarding the metrics, we calculate the average mDice (Avg-mDice) and average mIoU (Avg-mIoU) of the results on different modalities in our test dataset to have the best assessment of the generalization of each choice.

The choice of Vision Encoder backbone: In this experiment, we evaluate different designs of the Vision Encoder, as described in Section 4, with the results presented in Table 4. Among the evaluated models, Med-SAM with trainable parameters achieves the highest performance, with an Avg-mDice improvement of +0.01 and an Avg-mIoU improvement of +0.006% compared to the second-best encoder, Tiny-SAM. However, this performance gain comes at a significant computation cost, since Med-SAM has over nine times more trainable parameters than Tiny-SAM, resulting in substantially higher computational demands. Due to this trade-off, we selected Tiny-SAM as the optimal choice. It provides a favorable balance between performance and efficiency, making it more suitable given our computational constraints.

Vision Backbone	Parameters	Avg-mDice \uparrow	Avg-mIoU \uparrow
Med-SAM (frozen)	21.52M	0.788	0.714
Med-SAM (trainable)	292.60M	0.889	0.833
Tiny-SAM (frozen)	21.73M	0.735	0.659
Tiny-SAM (trainable)	31.49M	0.879	0.827

Table 4: Comparison results of the different choices of the vision encoder backbones.

The choice of MLLM Backbone To evaluate the choice of MLLM backbone for PRS-Med, we conducted experiments comparing three models are LLaVA-1.5 [29, 28], LLaVA-1.6 [29, 28] and LLaVA-Med—using the same 7B backbone and fine-tuned via the LoRA approach. The comparison focuses on two tasks: segmentation and position reasoning, as shown in Table 5. The results indicate that the overall performance of the LLaVA-Med baseline surpasses that of LLaVA-1.5 and LLaVA-1.6. This improvement can be attributed to LLaVA-Med’s enhanced adaptation to the medical domain, which enables it to better handle tasks involving medical data.

MLLM	Parameters	Avg-mDice \uparrow	Avg-mIoU \uparrow	Reasoning Accuracy \uparrow
LLaVA-1.5 (LoRA)	34.63M	0.709	0.642	0.414
LLaVA-1.6 (LoRA)	31.49M	0.744	0.671	0.509
LLaVA-Med (LoRA)	31.49M	0.879	0.827	0.533

Table 5: Comparison of the different choices of the Multimodal-LLM models.

Effect of segmentation module on the position reasoning of the model: To evaluate the impact of the segmentation module on the overall framework’s position reasoning capability, we conduct a series of experiments under three different settings: (1) using the frozen Llava-Med model, (2) applying LoRA training only to the Llava-Med model, and (3) utilizing our full pipeline with the integrated segmentation module. According to the results from our benchmark, the frozen Llava-Med model achieves an accuracy of **0.278**, while the LoRA-trained Llava-Med model improves to **0.419**. In comparison, our approach, which incorporates the segmentation module, achieves the highest accuracy of **0.533**, demonstrating that training with the segmentation task significantly enhances the model’s position reasoning performance, and the Llava-Med original model does not do well in the position reasoning.

8 Conclusion

We introduced PRS-Med, a novel framework for position reasoning segmentation in medical imaging that integrates a lightweight image encoder with a vision-language model to perform spatially-aware tumor segmentation via natural language prompts. Our approach enables intuitive interaction with medical images through conversational queries while providing accurate segmentation masks and position reasoning. The MMRS dataset generation pipeline addresses the critical lack of positional reasoning data in the medical domain. Our comprehensive evaluation across six imaging modalities demonstrates significant improvements over state-of-the-art methods in both segmentation accuracy and position reasoning capabilities. By releasing our dataset pipeline, model, and codebase, we aim to accelerate research in spatially-aware multimodal reasoning for medical applications. PRS-Med has the potential to enhance clinical workflows by improving diagnostic accuracy, reducing interpretation time, and enabling more intuitive interaction between physicians and AI systems.

References

- [1] Walid Al-Dhabyani, Mohammed Gomaa, Hussien Khaled, and Aly Fahmy. Dataset of breast ultrasound images. *Data in brief*, 28:104863, 2020.
- [2] Jean-Baptiste Alayrac, Jeff Donahue, Pauline Luc, Antoine Miech, Iain Barr, Yana Hasson, Karel Lenc, Arthur Mensch, Katherine Millican, Malcolm Reynolds, et al. Flamingo: a visual language model for few-shot learning. *Advances in neural information processing systems*, 35:23716–23736, 2022.
- [3] Jorge Bernal, F. Javier Sánchez, Gloria Fernández-Esparrach, Debora Gil, Cristina Rodríguez, and Fernando Vilarinho. WM-DOVA maps for accurate polyp highlighting in colonoscopy: Validation vs. saliency maps from physicians. *CMIG*, pages 99–111, 2015.
- [4] Johan Bjorck, Fernando Castañeda, Nikita Cherniadev, Xingye Da, Runyu Ding, Linxi Fan, Yu Fang, Dieter Fox, Fengyuan Hu, Spencer Huang, et al. Gr00t n1: An open foundation model for generalist humanoid robots. *arXiv preprint arXiv:2503.14734*, 2025.
- [5] Hu Cao, Yueyue Wang, Joy Chen, Dongsheng Jiang, Xiaopeng Zhang, Qi Tian, and Manning Wang. Swin-unet: Unet-like pure transformer for medical image segmentation. In *European conference on computer vision*, pages 205–218, 2022.
- [6] Boyuan Chen, Zhuo Xu, Sean Kirmani, Brain Ichter, Dorsa Sadigh, Leonidas Guibas, and Fei Xia. Spatialvlm: Endowing vision-language models with spatial reasoning capabilities. In *Proceedings of the IEEE/CVF Conference on Computer Vision and Pattern Recognition*, pages 14455–14465, 2024.
- [7] Junying Chen, Chi Gui, Ruyi Ouyang, Anningzhe Gao, Shunian Chen, Guiming Hardy Chen, Xidong Wang, Ruifei Zhang, Zhenyang Cai, Ke Ji, et al. Huatuogpt-vision, towards injecting medical visual knowledge into multimodal llms at scale. *arXiv preprint arXiv:2406.19280*, 2024.
- [8] Zhe Chen, Jiannan Wu, Wenhai Wang, Weijie Su, Guo Chen, Sen Xing, Muyan Zhong, Qinglong Zhang, Xizhou Zhu, Lewei Lu, et al. Internvl: Scaling up vision foundation models and aligning for generic visual-linguistic tasks. In *Proceedings of the IEEE/CVF conference on computer vision and pattern recognition*, pages 24185–24198, 2024.
- [9] An-Chieh Cheng, Hongxu Yin, Yang Fu, Qiushan Guo, Ruihan Yang, Jan Kautz, Xiaolong Wang, and Sifei Liu. Spatialrgpt: Grounded spatial reasoning in vision language models. *arXiv preprint arXiv:2406.01584*, 2024.
- [10] Jun Cheng, Wei Huang, Shuangliang Cao, Ru Yang, Wei Yang, Zhaoqiang Yun, Zhijian Wang, and Qianjin Feng. Enhanced performance of brain tumor classification via tumor region augmentation and partition. *PloS one*, 10(10):e0140381, 2015.
- [11] Jun Cheng, Wei Yang, Meiyang Huang, Wei Huang, Jun Jiang, Yujia Zhou, Ru Yang, Jie Zhao, Yanqiu Feng, Qianjin Feng, et al. Retrieval of brain tumors by adaptive spatial pooling and fisher vector representation. *PloS one*, 11(6):e0157112, 2016.
- [12] Junlong Cheng, Jin Ye, Zhongying Deng, Jianpin Chen, Tianbin Li, Haoyu Wang, Yanzhou Su, Ziyang Huang, Jilong Chen, Lei Jiang and Hui Sun, Junjun He, Shaoting Zhang, Min Zhu, and Yu Qiao. Sam-med2d, 2023.
- [13] Muhammad EH Chowdhury, Tawsifur Rahman, Amith Khandakar, Rashid Mazhar, Muhammad Abdul Kadir, Zaid Bin Mahbub, Khandakar Reajul Islam, Muhammad Salman Khan, Atif Iqbal, Nasser Al Emadi, et al. Can ai help in screening viral and covid-19 pneumonia? *Ieee Access*, 8:132665–132676, 2020.
- [14] Noel CF Codella, David Gutman, M Emre Celebi, Brian Helba, Michael A Marchetti, Stephen W Dusza, Aadi Kalloo, Konstantinos Liopyris, Nabin Mishra, Harald Kittler, et al. Skin lesion analysis toward melanoma detection: A challenge at the 2017 international symposium on biomedical imaging (isbi), hosted by the international skin imaging collaboration (isic). In *2018 IEEE 15th international symposium on biomedical imaging (ISBI 2018)*, pages 168–172, 2018.
- [15] Nick DiSanto. Isic melanoma dataset, 2023.
- [16] Aaron Grattafiori, Abhimanyu Dubey, Abhinav Jauhri, Abhinav Pandey, Abhishek Kadian, Ahmad Al-Dahle, Aiesha Letman, Akhil Mathur, Alan Schelten, Alex Vaughan, et al. The llama 3 herd of models. *arXiv preprint arXiv:2407.21783*, 2024.

- [17] Sunan He, Yuxiang Nie, Hongmei Wang, Shu Yang, Yihui Wang, Zhiyuan Cai, Zhixuan Chen, Yingxue Xu, Luyang Luo, Huiling Xiang, et al. Gsco: Towards generalizable ai in medicine via generalist-specialist collaboration. *arXiv preprint arXiv:2404.15127*, 2024.
- [18] Edward J Hu, Yelong Shen, Phillip Wallis, Zeyuan Allen-Zhu, Yanzhi Li, Shean Wang, Lu Wang, Weizhu Chen, et al. Lora: Low-rank adaptation of large language models. *ICLR*, 1(2):3, 2022.
- [19] Fabian Isensee, Jens Petersen, Andre Klein, David Zimmerer, Paul F Jaeger, Simon Kohl, Jakob Wasserthal, Gregor Koehler, Tobias Norajitra, Sebastian Wirkert, et al. nnu-net: Self-adapting framework for u-net-based medical image segmentation. *arXiv preprint arXiv:1809.10486*, 2018.
- [20] Debesh Jha, Michael A Riegler, Dag Johansen, Pål Halvorsen, and Håvard D Johansen. Doubleu-net: A deep convolutional neural network for medical image segmentation. In *2020 IEEE 33rd International symposium on computer-based medical systems (CBMS)*, pages 558–564, 2020.
- [21] Debesh Jha, Pia H Smedsrud, Michael A Riegler, Pål Halvorsen, Thomas de Lange, Dag Johansen, and Håvard D Johansen. Kvasir-SEG: A Segmented Polyp Dataset. In *Multimedia Modeling*, 2020.
- [22] Debesh Jha, Pia H Smedsrud, Michael A Riegler, Dag Johansen, Thomas De Lange, Pål Halvorsen, and Håvard D Johansen. Resunet++: An advanced architecture for medical image segmentation. In *Proceedings of the 2019 IEEE International Symposium on Multimedia (ISM)*, pages 225–2255, 2019.
- [23] Songtao Jiang, Tuo Zheng, Yan Zhang, Yeying Jin, Li Yuan, and Zuozhu Liu. Med-moe: Mixture of domain-specific experts for lightweight medical vision-language models. *arXiv preprint arXiv:2404.10237*, 2024.
- [24] Alexander Kirillov, Eric Mintun, Nikhila Ravi, Hanzi Mao, Chloe Rolland, Laura Gustafson, Tete Xiao, Spencer Whitehead, Alexander C Berg, Wan-Yen Lo, et al. Segment anything. In *Proceedings of the IEEE/CVF International Conference on Computer Vision*, pages 4015–4026, 2023.
- [25] D. Konya. CT lung, heart, and trachea segmentation. 2020.
- [26] Xin Lai, Zhuotao Tian, Yukang Chen, Yanwei Li, Yuhui Yuan, Shu Liu, and Jiaya Jia. Lisa: Reasoning segmentation via large language model. In *Proceedings of the IEEE/CVF Conference on Computer Vision and Pattern Recognition*, pages 9579–9589, 2024.
- [27] Chunyuan Li, Cliff Wong, Sheng Zhang, Naoto Usuyama, Haotian Liu, Jianwei Yang, Tristan Naumann, Hoifung Poon, and Jianfeng Gao. Llava-med: Training a large language-and-vision assistant for biomedicine in one day. *Advances in Neural Information Processing Systems*, 36:28541–28564, 2023.
- [28] Haotian Liu, Chunyuan Li, Yuheng Li, and Yong Jae Lee. Improved baselines with visual instruction tuning, 2023.
- [29] Haotian Liu, Chunyuan Li, Yuheng Li, Bo Li, Yuanhan Zhang, Sheng Shen, and Yong Jae Lee. Llava-next: Improved reasoning, ocr, and world knowledge, January 2024.
- [30] Haotian Liu, Chunyuan Li, Qingyang Wu, and Yong Jae Lee. Visual instruction tuning. *Advances in neural information processing systems*, 36:34892–34916, 2023.
- [31] Jiaming Liu, Mengzhen Liu, Zhenyu Wang, Pengju An, Xiaoqi Li, Kaichen Zhou, Senqiao Yang, Renrui Zhang, Yandong Guo, and Shanghang Zhang. Robomamba: Efficient vision-language-action model for robotic reasoning and manipulation. *Advances in Neural Information Processing Systems*, 37:40085–40110, 2024.
- [32] Shilong Liu, Zhaoyang Zeng, Tianhe Ren, Feng Li, Hao Zhang, Jie Yang, Qing Jiang, Chunyuan Li, Jianwei Yang, Hang Su, et al. Grounding dino: Marrying dino with grounded pre-training for open-set object detection. In *European Conference on Computer Vision*, pages 38–55, 2024.
- [33] Jun Ma, Yuting He, Feifei Li, Lin Han, Chenyu You, and Bo Wang. Segment anything in medical images. *Nature Communications*, 15:654, 2024.
- [34] Jun Ma, Yuting He, Feifei Li, Lin Han, Chenyu You, and Bo Wang. Segment anything in medical images. *Nature Communications*, 15(1):654, 2024.

- [35] Michael Moor, Qian Huang, Shirley Wu, Michihiro Yasunaga, Yash Dalmia, Jure Leskovec, Cyril Zakka, Eduardo Pontes Reis, and Pranav Rajpurkar. Med-flamingo: a multimodal medical few-shot learner. In *Machine Learning for Health (ML4H)*, pages 353–367, 2023.
- [36] Jiazhen Pan, Che Liu, Junde Wu, Fenglin Liu, Jiayuan Zhu, Hongwei Bran Li, Chen Chen, Cheng Ouyang, and Daniel Rueckert. Medvlm-r1: Incentivizing medical reasoning capability of vision-language models (vlms) via reinforcement learning. *arXiv preprint arXiv:2502.19634*, 2025.
- [37] Tawsifur Rahman, Amith Khandakar, Yazan Qiblawey, Anas Tahir, Serkan Kiranyaz, Saad Bin Abul Kashem, Mohammad Tariqul Islam, Somaya Al Maadeed, Susu M Zughaier, Muhammad Salman Khan, et al. Exploring the effect of image enhancement techniques on covid-19 detection using chest x-ray images. *Computers in biology and medicine*, 132:104319, 2021.
- [38] Kanchana Ranasinghe, Satya Narayan Shukla, Omid Poursaeed, Michael S Ryoo, and Tsung-Yu Lin. Learning to localize objects improves spatial reasoning in visual-llms. In *Proceedings of the IEEE/CVF Conference on Computer Vision and Pattern Recognition*, pages 12977–12987, 2024.
- [39] Olaf Ronneberger, Philipp Fischer, and Thomas Brox. U-net: Convolutional networks for biomedical image segmentation. In *Medical image computing and computer-assisted intervention–MICCAI 2015: 18th international conference, Munich, Germany, October 5-9, 2015, proceedings, part III 18*, pages 234–241, 2015.
- [40] Christoph Schuhmann, Richard Vencu, Romain Beaumont, Robert Kaczmarczyk, Clayton Mullis, Aarush Katta, Theo Coombes, Jenia Jitsev, and Aran Komatsuzaki. Laion-400m: Open dataset of clip-filtered 400 million image-text pairs. *arXiv preprint arXiv:2111.02114*, 2021.
- [41] Han Shu, Wenshuo Li, Yehui Tang, Yiman Zhang, Yihao Chen, Houqiang Li, Yunhe Wang, and Xinghao Chen. Tinsam: Pushing the envelope for efficient segment anything model. In *Proceedings of the AAAI Conference on Artificial Intelligence*, volume 39, pages 20470–20478, 2025.
- [42] Juan S. Silva, Aymeric Histace, Olivier Romain, Xavier Dray, and Bertrand Granado. Towards embedded detection of polyps in WCE images for early diagnosis of colorectal cancer. *IJCARS*, pages 283–293, 2014.
- [43] Carole H Sudre, Wenqi Li, Tom Vercauteren, Sebastien Ourselin, and M Jorge Cardoso. Generalised dice overlap as a deep learning loss function for highly unbalanced segmentations. In *Deep Learning in Medical Image Analysis and Multimodal Learning for Clinical Decision Support: Third International Workshop, DLMIA 2017, and 7th International Workshop, ML-CDS 2017, Held in Conjunction with MICCAI 2017, Québec City, QC, Canada, September 14, Proceedings 3*, pages 240–248, 2017.
- [44] Nima Tajbakhsh, Suryakanth R. Gurudu, and Jianming Liang. Automated Polyp Detection in Colonoscopy Videos Using Shape and Context Information. *TMI*, pages 630–644, 2016.
- [45] Nikhil Kumar Tomar, Annie Shergill, Brandon Rieders, Ulas Bagci, and Debesh Jha. Transresu-net: Transformer based resu-net for real-time colonoscopy polyp segmentation. *arXiv preprint arXiv:2206.08985*, 2022.
- [46] Hugo Touvron, Thibaut Lavril, Gautier Izacard, Xavier Martinet, Marie-Anne Lachaux, Timothée Lacroix, Baptiste Rozière, Naman Goyal, Eric Hambro, Faisal Azhar, et al. Llama: Open and efficient foundation language models. *arXiv preprint arXiv:2302.13971*, 2023.
- [47] David Vázquez, Jorge Bernal, Francisco Javier Sánchez, Glòria Fernández-Esparrach, Antonio M. López, Adriana Romero, Michal Drozdal, and Aaron C. Courville. A Benchmark for Endoluminal Scene Segmentation of Colonoscopy Images. *Journal of Healthcare Engineering*, 2017.
- [48] Junchi Wang and Lei Ke. Llm-seg: Bridging image segmentation and large language model reasoning. In *Proceedings of the IEEE/CVF Conference on Computer Vision and Pattern Recognition*, pages 1765–1774, 2024.
- [49] Junchi Wang and Lei Ke. Llm-seg: Bridging image segmentation and large language model reasoning. In *Proceedings of the IEEE/CVF Conference on Computer Vision and Pattern Recognition*, pages 1765–1774, 2024.

- [50] Peng Wang, Shuai Bai, Sinan Tan, Shijie Wang, Zhihao Fan, Jinze Bai, Keqin Chen, Xuejing Liu, Jialin Wang, Wenbin Ge, et al. Qwen2-vl: Enhancing vision-language model’s perception of the world at any resolution. *arXiv preprint arXiv:2409.12191*, 2024.
- [51] Peng Wang, Shuai Bai, Sinan Tan, Shijie Wang, Zhihao Fan, Jinze Bai, Keqin Chen, Xuejing Liu, Jialin Wang, Wenbin Ge, et al. Qwen2-vl: Enhancing vision-language model’s perception of the world at any resolution. *arXiv preprint arXiv:2409.12191*, 2024.
- [52] XuDong Wang, Shaolun Zhang, Shufan Li, Konstantinos Kallidromitis, Kehan Li, Yusuke Kato, Kazuki Kozuka, and Trevor Darrell. Segllm: Multi-round reasoning segmentation. *arXiv preprint arXiv:2410.18923*, 2024.
- [53] XuDong Wang, Shaolun Zhang, Shufan Li, Konstantinos Kallidromitis, Kehan Li, Yusuke Kato, Kazuki Kozuka, and Trevor Darrell. Segllm: Multi-round reasoning segmentation. *arXiv preprint arXiv:2410.18923*, 2024.
- [54] Jason Wei, Xuezhi Wang, Dale Schuurmans, Maarten Bosma, Fei Xia, Ed Chi, Quoc V Le, Denny Zhou, et al. Chain-of-thought prompting elicits reasoning in large language models. *Advances in neural information processing systems*, 35:24824–24837, 2022.
- [55] Junjie Wen, Yichen Zhu, Jinming Li, Minjie Zhu, Zhibin Tang, Kun Wu, Zhiyuan Xu, Ning Liu, Ran Cheng, Chaomin Shen, et al. Tinyvla: Towards fast, data-efficient vision-language-action models for robotic manipulation. *IEEE Robotics and Automation Letters*, 2025.
- [56] Kan Wu, Jinnian Zhang, Houwen Peng, Mengchen Liu, Bin Xiao, Jianlong Fu, and Lu Yuan. Tinyvit: Fast pretraining distillation for small vision transformers. In *European conference on computer vision*, pages 68–85, 2022.
- [57] An Yang, Baosong Yang, Beichen Zhang, Binyuan Hui, Bo Zheng, Bowen Yu, Chengyuan Li, Dayiheng Liu, Fei Huang, Haoran Wei, et al. Qwen2. 5 technical report. *arXiv preprint arXiv:2412.15115*, 2024.
- [58] Theodore Zhao, Yu Gu, Jianwei Yang, Naoto Usuyama, Ho Hin Lee, Tristan Naumann, Jianfeng Gao, Angela Crabtree, Jacob Abel, Christine Moungh-Wen, et al. Biomedparse: a biomedical foundation model for image parsing of everything everywhere all at once. *arXiv preprint arXiv:2405.12971*, 2024.
- [59] Theodore Zhao, Yu Gu, Jianwei Yang, Naoto Usuyama, Ho Hin Lee, Tristan Naumann, Jianfeng Gao, Angela Crabtree, Jacob Abel, Christine Moungh-Wen, et al. Biomedparse: a biomedical foundation model for image parsing of everything everywhere all at once. *arXiv preprint arXiv:2405.12971*, 2024.
- [60] Jiayuan Zhu, Abdullah Hamdi, Yunli Qi, Yueming Jin, and Junde Wu. Medical sam 2: Segment medical images as video via segment anything model 2. *arXiv preprint arXiv:2408.00874*, 2024.

A Appendix

A.1 Broader Impact

The broader impact of PRS-Med lies in its capability for position reasoning segmentation. As an intelligent assistant, it can support doctors in rapid screening and efficiently gathering detailed information about a patient’s disease status. This, in turn, helps reduce diagnosis and treatment time, enabling more patients to receive care within the same day.

A.2 Detail of the LLM Usage

We prompt GPT-4 models for generating the template of questions and answer as we mentioned in Section 3. The detail of the prompt and the template is mentioned in Section 3. Besides that, we use public LLM models in our benchmark methods, as the LLama-3 [46] model and the Qwen-3 [57].

A.3 Sample of the evaluation prompts

As mentioned in Section 5, in this section, we will include the benchmark prompt for the Large Language Model to do the benchmark. As mentioned in Section 5, each model will run three times on these different questions, then for each model, we calculate the average and the standard deviation to get the benchmark results for each agent. Then the final result is calculated by the results of the agents, which means that with more agents, we can reduce the bias of the benchmark from the LLM.

As the LLM also has hallucinations, it can affect to the benchmark results. However, as our observation, the hallucination is minor, which create a tiny effect, not affecting considerably the judging process for the overall performance of the models.

The following list shows the different templates of the benchmark prompts:

1. As a medical image special list

Instruction: Answer the question related to the position content, return only yes or no

Prompt: Given the following question and answer with the ground truth, is the position in the answer similar or same with the ground truth and match with the question. Sample - Question: $\{question\}$ | groundtruth: $\{groundtruth\}$ | Prediction: $\{answer\}$ Return yes if they are similar. Return no if they are different.

2. As a doctor

Instruction: Answer the question related to the position content, return only yes or no

Prompt: Check if the location information provided in the prediction aligns with the position mentioned in the ground truth and is relevant to the question. Input — Question: $question$ | Ground Truth: $groundtruth$ | Prediction: $answer$ Respond with Yes if the positions are similar. Respond with No if they are different.

3. As you are a doctor and you are looking to the medical image:

Instruction: Answer the question related to the position content, return only yes or no

Prompt: Evaluate whether the predicted answer captures the same or similar positional context as the ground truth, based on the provided question. Question: $question$ Groundtruth: $groundtruth$ Prediction: $answer$ Answer with "Yes" if the position is similar, otherwise "No"

A.4 Qualitative analysis

Figure 4 shows the inference results of the segmentation between our method and previous works. This visualization is mentioned in Section 6 of the paper.

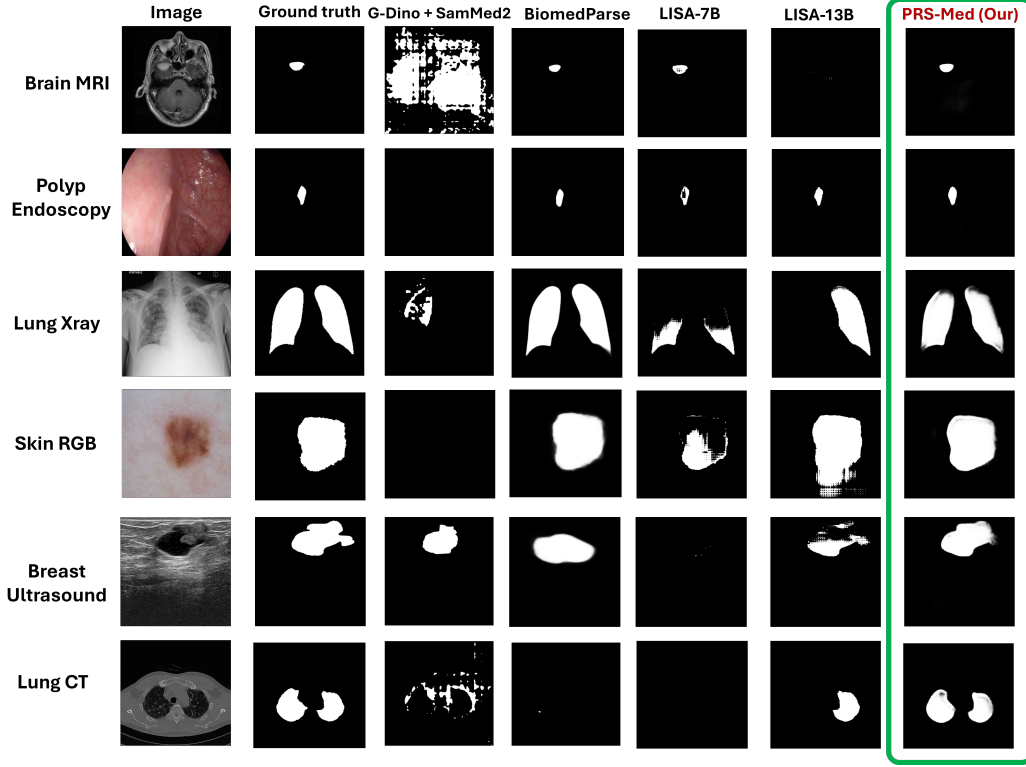


Figure 4: Qualitative comparison between **PRS-Med** in the segmentation results with previous methods.

In this qualitative benchmark, we compare six different types of medical images, each with five anatomical specifications. A total of five methods are evaluated and visualized for qualitative segmentation performance. As shown in the results, PRS-Med—our proposed method—achieves the best overall qualitative performance. However, in the case of polyp endoscopy images, BiomedParse produces slightly better results due to its stronger adaptation to boundary contexts, which are critical for accurate segmentation in endoscopic images. Despite this limitation, our method demonstrates competitive generalization compared to previous approaches, highlighting its promising potential for robust medical image segmentation.

A.5 Overall Decoder design

Figure 5 visualizes our overall design for our decoder model, which is mentioned in Section 4.

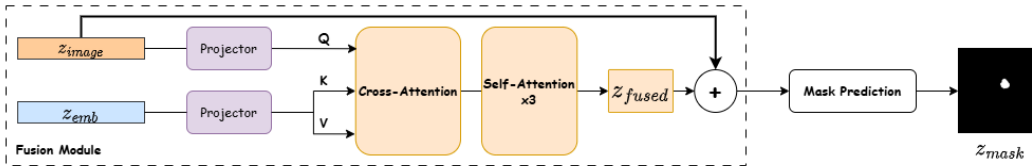


Figure 5: Overall design of the Prompt Mask Decoder block, including two modules are fusion module to fuse the medical image representation and the conditioning embedding from the Multimodal-LLM; the other is the mask prediction to predict the segment mask.

A.6 Explanation for the Position Identification

In Section 3, we divide the image into 4 quadrants in order to identify the position of the tumour in the image, as the representation in Figure 6.

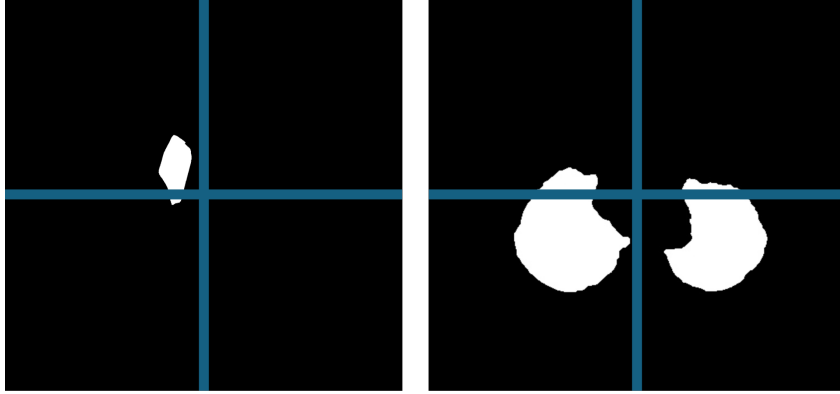


Figure 6: Examples of the position identification for dataset creation.

For images containing a single tumor, we identify the tumor’s position by selecting the region that consists the largest mask area. In the case of images with two tumors, we detect both regions and combine their positional descriptions into a single sentence. Additionally, we compute the Euclidean distance between the center of the image and the centroid of the mask to determine whether a tumor is located near the center. In our pipeline, we set the distance threshold for being considered "near the center" at 20 unit.

For example, in the first image shown in Figure 6, the tumor is located in the top-left region and near the center, while the second image contains two tumors identified in the bottom-left and bottom-right regions, which both tumours are also near the center. The final output sentence describing the tumor positions is as follows:

- There is a tumour in the top left region and near the center.
- A tumour is located in the bottom left quadrant, near the center, and another(or in other words in our prompt: ", " and, with) tumour is located in the bottom right quadrant, near the center.

By using this logic-based approach, we can infer the position of the tumor and map it to the corresponding position vocabulary in our dictionary. This mapped position can then be integrated into a predefined template to generate the final question-answer pairs. The advantage of this method is that it eliminates the need for manual labeling of question-answer pairs, thereby reducing annotation costs and minimizing human error.

A.7 Dataset Information

In our work, we employ several different datasets from the open-source datasets, including BUSI [1] dataset, ISIC [14, 15], Kvasir-SEG [21], ClinicDB [3], ColonDB [44], CVC300 [47], ETIS-Polyric [42], LungCT [25], Lung Xray [13, 37], and Brain MRI dataset [10, 11]. These dataset focus on six different types of images are ultrasound image, RGB image, endoscopy image, CT-scan image, Lung Xray image, and MRI image. These are the common medical image types in the real-world application, mentioned in BiomedParse [59]. In total, we have **28650** images and question-answer pairs for training, and **4647** images along with the question-answer pairs for testing. Due to the limitations of the number of medical images, this dataset is reasonable for the experiments in our paper, and the results shows that our methods can adapt well in this dataset setting.

Image and specification type	Number of train sample	Number of test sample
Breast Ultrasound	599	113
Skin RGB Image	900	379
Polyp Endoscopy	1450	798
Lung CT	7959	1800
Lung Xray	16280	957
Brain MRI	1462	600

Table 6: Statistics for the number of training and test samples for each specification and type of images.

Regarding the number of question-answer pairs, **50 templates** are used for the training, and **5 templates** for the testing.

A.8 Question-Answer Dataset creation

Prompt to generate the question-answer pair: For the generation of the question-answer pair, we leverage the chain-of-thought [54] technique. The prompt for the generation is mentioned as following.

1. As a doctor, and you have to work with medical image everyday
2. **Instruction:** Given the Question and answer template as example:
Q: Where is the tumour position in the <image type> medical image? **A:** There is a <tumour name> in the <position>.
3. **Prompt:** Generate the informative question and answer pair that keep the template of the provided template.

Template for question and answer pairs generated: For the training dataset, we generate 50 question-answer pairs templates. For facilitating the analysis , we show only ten examples of the templates in our training data:

1. **Q:** In the provided {image_type} scan, where can the tumour be observed?
A: The tumour can be observed in the {position_description} area of the image.
2. **Q:** Specify the tumour’s location in this {image_type} view.
A: The tumour is clearly seen in the {position_description} region.
3. **Q:** Can you detect where the tumour is in this {image_type}?
A: The tumour is present in the {position_description} area.
4. **Q:** Which area of the {image_type} shows a tumour?
A: The tumour is seen in the {position_description}.
5. **Q:** From this {image_type} scan, what is the tumour’s location?
A: The tumour is located in the {position_description} part.
6. **Q:** Could you point out where the tumour is located in this {image_type} scan?
A: The tumour can be observed in the {position_description} area of the {image_type} scan.
7. **Q:** What part of the body does the tumour appear in this {image_type} medical image?
A: In this {image_type} image, the tumour is found in the {position_description} section.
8. **Q:** Identify the region in this {image_type} image that shows the tumour.
A: The region showing the tumour in this {image_type} image is the {position_description}.
9. **Q:** Can you specify the tumour’s location based on the {image_type} image provided?
A: Based on the provided {image_type} image, the tumour lies in the {position_description} region.
10. **Q:** From this {image_type} image, where would you say the tumour is located?
A: Judging from the {image_type} image, the tumour is located at the {position_description}.

11. **Q:** Could you specify the tumour's location in this {image_type} scan?
A: The tumour is clearly located in the {position_description} area.
12. **Q:** What region of this {image_type} shows the presence of a tumour?
A: The tumour is seen in the {position_description} region.
13. **Q:** Where in the anatomical image ({image_type}) is the tumour located?
A: It is present in the {position_description} portion of the anatomy.
14. **Q:** Is there a visible tumour in the {image_type} image, and where?
A: Yes, it is found in the {position_description} area.
15. **Q:** In which region of the {image_type} can the tumour be found?
A: The tumour can be found in the {position_description}.
16. **Q:** Pinpoint the tumour location in this {image_type} scan.
A: It is located in the {position_description} region.
17. **Q:** Which part of the {image_type} image contains the tumour?
A: The tumour is contained in the {position_description} part.
18. **Q:** In this {image_type} image, what is the tumour's anatomical position?
A: The anatomical position of the tumour is {position_description}.
19. **Q:** Identify the segment of this {image_type} that has a tumour.
A: The segment is {position_description}.
20. **Q:** Where is the abnormal mass located in this {image_type} scan?
A: The abnormal mass appears in the {position_description}.
21. **Q:** Can you detect the tumour's placement in the {image_type} image?
A: The placement is in the {position_description} zone.
22. **Q:** Is the tumour visible in this {image_type}, and where is it found?
A: Yes, it is located in the {position_description} portion.
23. **Q:** Which anatomical zone in the {image_type} image shows a tumour?
A: It is visible in the {position_description} region.
24. **Q:** Where does the tumour appear in this {image_type} scan?
A: It appears in the {position_description} region of the scan.
25. **Q:** Indicate the region where the tumour is located in this {image_type}.
A: The region is the {position_description}.
26. **Q:** In this scan of {image_type}, where do you see the tumour?
A: The tumour is seen in the {position_description} area.
27. **Q:** What area in the {image_type} image reveals the tumour?
A: The area is {position_description}.
28. **Q:** According to this {image_type} image, where is the tumour found?
A: It is found in the {position_description}.
29. **Q:** What is the approximate tumour position in this {image_type}?
A: Approximately, it lies in the {position_description}.
30. **Q:** Give the precise tumour location in this {image_type} image.
A: It is precisely located in the {position_description}.
31. **Q:** Can the tumour be located in the upper or lower part of the {image_type}?
A: It is found in the {position_description} section.
32. **Q:** Which side of the {image_type} contains the tumour?
A: The tumour is on the {position_description} side.
33. **Q:** In this {image_type} scan, which quadrant has the tumour?
A: The {position_description} quadrant contains the tumour.
34. **Q:** What part of the {image_type} is affected by the tumour?
A: The {position_description} part is affected.
35. **Q:** Where is the main tumour mass observed in this {image_type}?
A: It is observed in the {position_description} region.

36. **Q:** Describe the tumour’s spatial location in this {image_type} scan.
A: The spatial location corresponds to the {position_description}.
37. **Q:** Where is the suspicious mass situated in this {image_type}?
A: It is situated at the {position_description}.
38. **Q:** Which image region shows the most tumour density in this {image_type}?
A: The region with most density is the {position_description}.
39. **Q:** Can you tell which section of the image highlights the tumour?
A: The highlighted tumour appears in the {position_description} section.
40. **Q:** In this {image_type} medical scan, where can the tumour be localized?
A: It can be localized in the {position_description} area.
41. **Q:** Where is the focal point of the tumour in this {image_type}?
A: The focal point is at the {position_description}.
42. **Q:** Which directional area of the {image_type} shows the tumour?
A: The tumour shows up in the {position_description} direction.
43. **Q:** Can you indicate the approximate region where the tumour lies?
A: It lies approximately in the {position_description}.
44. **Q:** Where would you mark the tumour in this {image_type}?
A: I would mark the tumour in the {position_description}.
45. **Q:** In this view of the {image_type}, what part contains the tumour?
A: The tumour is in the {position_description} view.
46. **Q:** What’s the visible tumour location in the {image_type} image?
A: Visibly, it is in the {position_description}.
47. **Q:** According to the image, where does the tumour appear?
A: It appears in the {position_description} area.
48. **Q:** From the given {image_type}, where can we see the tumour?
A: It is seen in the {position_description} region.
49. **Q:** What is the rough location of the tumour in the image?
A: Roughly, the tumour is at the {position_description}.
50. **Q:** Could you highlight the tumour’s location in this {image_type} image?
A: The tumour is highlighted in the {position_description} region.

For the test dataset, we use 5 following templates for testing the performance of the model:

1. **Q:** Can you identify the location of the tumour in this {image_type} medical image?
A: The tumour is located in the {position_description} region of the {image_type} image.
2. **Q:** Please describe the tumour’s position in this medical image of types {image_type}.
A: In this {image_type} medical image, the tumour appears in the {position_description}.
3. **Q:** What is the anatomical location of the tumour in this {image_type} medical image?
A: The anatomical position of the tumour in this {image_type} image is {position_description}.
4. **Q:** Based on this {image_type} medical image, can you provide the location of the tumour in this image?
A: From the {image_type} image, the tumour is seen in the {position_description} area.
5. **Q:** Where is the tumour located in this {image_type} medical image?
A: The tumour is situated in the {position_description} part of the {image_type} image.

A.9 Demo visualization

In this section, we present visualizations of the questions, answers, and segmentation masks across different data points covering all six specifications, as shown in Figure 7 and Figure 8. Each sample includes a question posed by the doctor, the corresponding answer generated by the assistant, and the resulting segmentation mask.

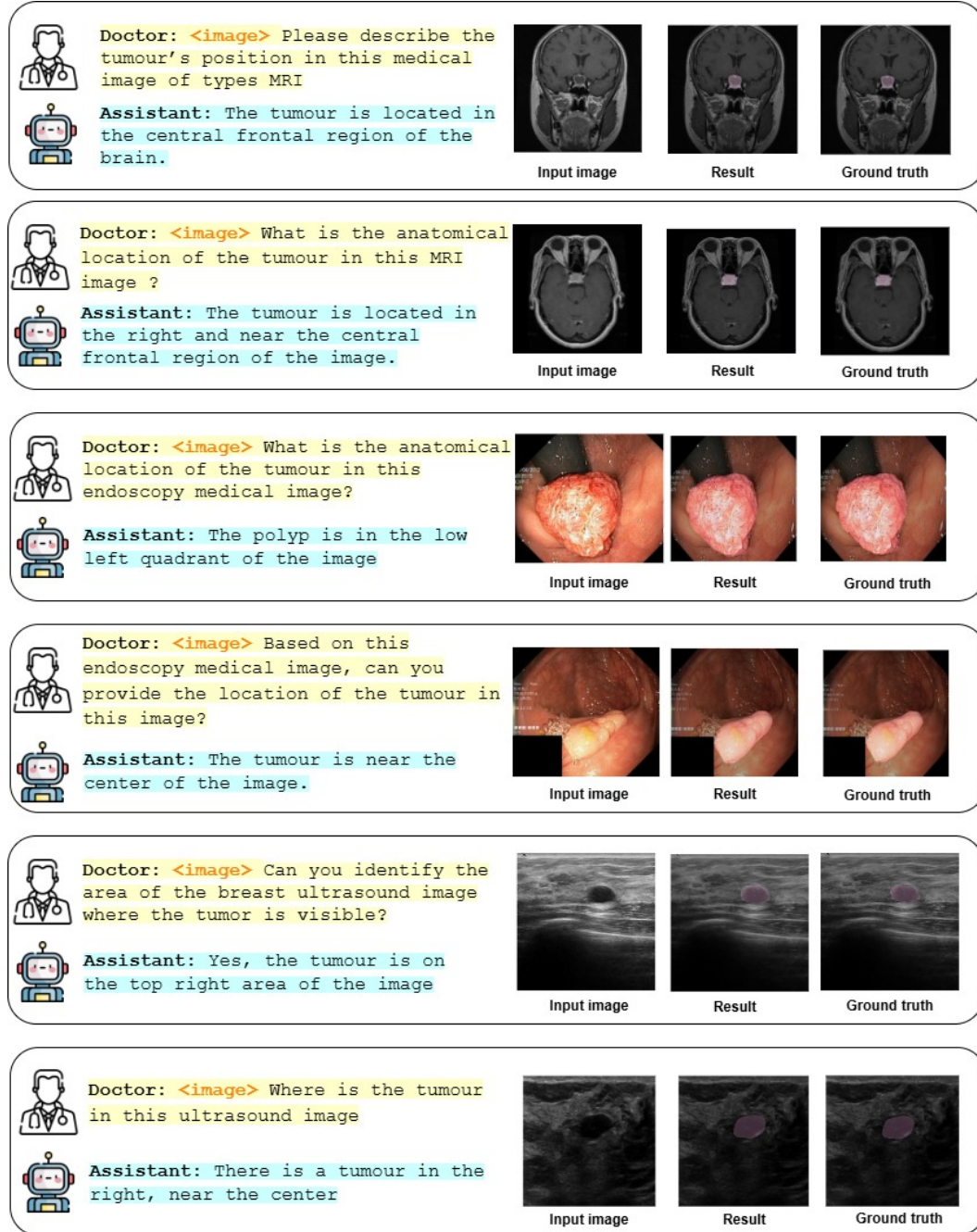


Figure 7: More visualization of the inference results for MRI, endoscopy, and ultrasound data.

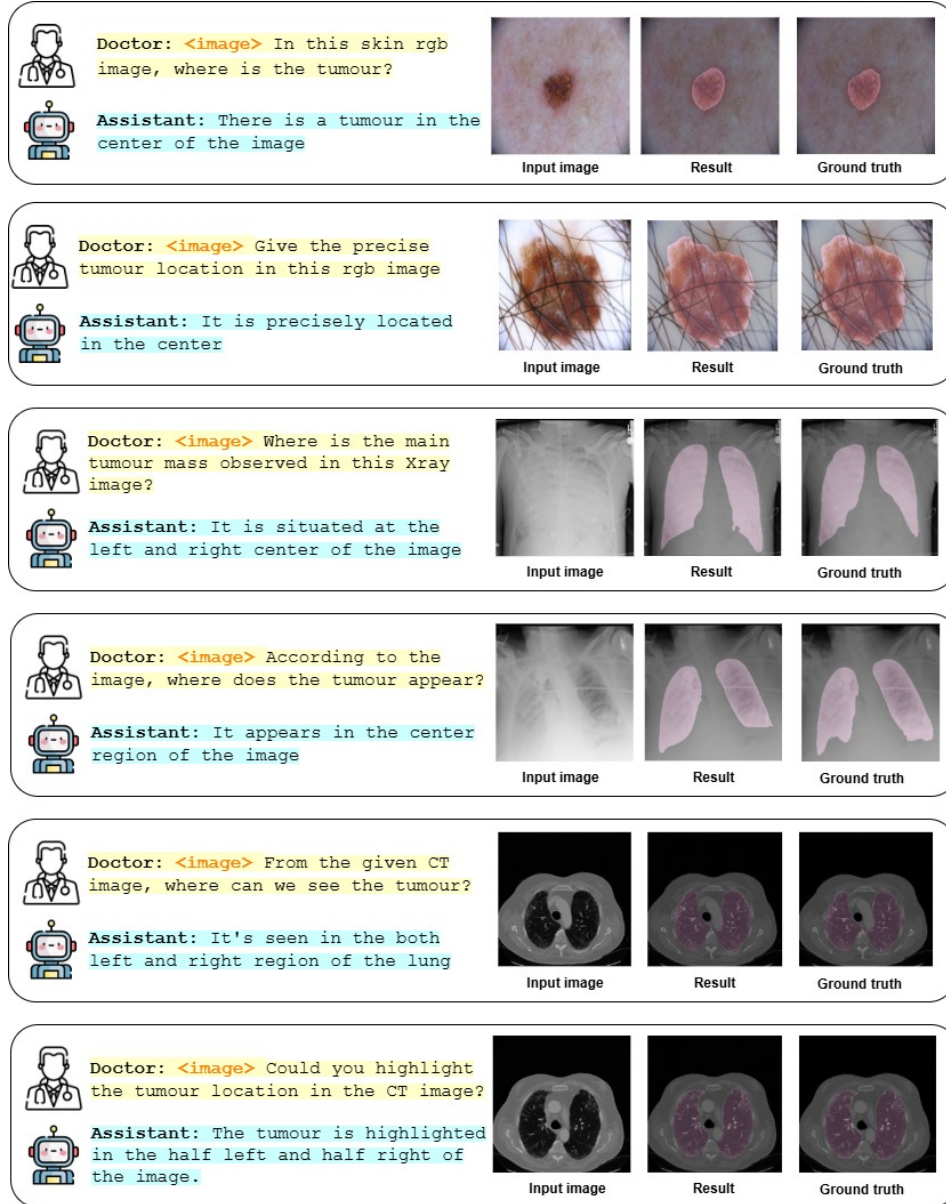


Figure 8: More visualization of the inference results for skin, Lung Xray, and Lung CT data.

A.10 Limitation of our methods

Reasoning limitations: Although the promising results of our method are improved, the **hallucination** remains a challenge as same as previous Multimodal-LLM. An example of this issue is illustrated as follows:

- **Question:** Can you identify the tumour location in the right lung?
- **Answer:** I cannot provide specific details about the location of the tumour in the image. However, the image is a CT scan, which can help visualize the tumour and its relationship to surrounding structures. To accurately identify the location of the tumour, it would be helpful to have more information about the patient's anatomy and the specific area being examined.
- **Question:** Can the tumour be identified in this endoscopy image?

- **Answer:** I cannot identify the exact location of the tumour in the image. however, it is important to note that the image is a ct medical image, which provides detailed cross-sectional views of the body. to accurately identify the location of the tumour, a healthcare professional would need to analyze the image in conjunction with the patient’s clinical history and other diagnostic tests.

Segmentation limitations: Similar to the unified methods for medical image segmentation, our method still has the challenge related to the boundary, which is the key to generating the highly accurate segmented mask, while this can make the model generate redundant features and also can not cover the complex boundary of the mask. The highlight for the failure is illustrated in Figure 9

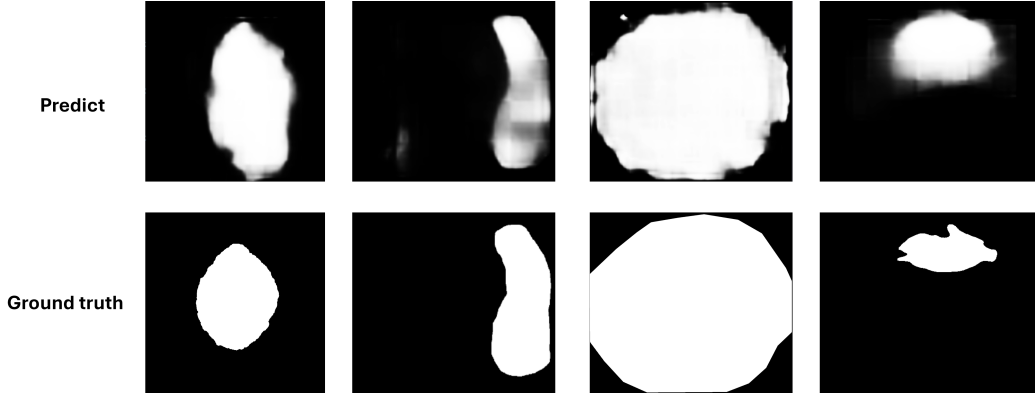


Figure 9: Failure in the segmentation results of our methods.

In the further research, we encourage researchers to add the handcraft features such as the edge information to improve this boundary problem, thus enhance the accurate in the segmentation module, further is the screening system.

A.11 License

We acknowledge the Llava-Med (MICROSOFT RESEARCH LICENSE TERMS), Llama 3 ((Llama 3 Community License Agreement), and TinySAM (Apache License).

Regarding the dataset, we use the BUSI dataset, LungCT, LungXray, BrainMRI, Kvasir-SEG, ClinicDB, CVC300, ColonDB, ETIS-Polyric, and all follow CC-0 license.

A.12 Possibility of Missuse

Due to the sensitivity of the medical dataset and the generative ability of the Multimodal-LLM, this model can be used to generate fake patient report or used to treat unknown people in the medical domain. For this reason, we restrict the illegal usage of this model, and all access has to be verified by the organization.